Chapter 8

Dynamics of two coupled Bose gas modes

The next step up towards a many-mode simulation is to see how the statistical behavior of the gauge methods is affected once mode mixing occurs. In this chapter, the effect of the combined drift and diffusion gauges suggested in Section 7.10 on dynamical simulations of a two-mode system will be considered (undamped, gainless, with two modes coupled by Rabi oscillations). This system is simple enough that there are only a few parameters, yet many of the changes caused by mode mixing are visible.

8.1 The model

The system consists of two orthogonal modes labeled 1 and 2 with interparticle interactions in each mode, and Rabi coupling between them. The coupling frequency will be restricted to be real for simplicity (complex values can always be considered in similar vein with no significant alterations to the following discussion). Time units are chosen so that the nonlinear interaction frequency is $\chi = 1$, and a transformation is made to an interaction picture in which the linear mode self-energies $\hbar\omega_{jj}\widehat{n}_j$ are moved into the Heisenberg evolution of operators. The interaction picture

Hamiltonian then is

$$\widehat{H} = \hbar\omega_{12}\left[\widehat{a}_1^\dagger\widehat{a}_2 + \widehat{a}_2^\dagger\widehat{a}_1\right] + \hbar\sum_{j=1}^{2}\widehat{a}_j^{\dagger 2}\widehat{a}_j^2. \tag{8.1}$$

The Rabi frequency is ω_{12} (in scaled time units).

Physically this model can represent, for example, a simplified model of two internal boson states coupled by an EM field, or two trapped condensates spatially separated by a barrier. This approximation has been used by a multitude of authors to investigate the quantum behavior of BECs in two-state systems. For references to some of the work in this field see Leggett [30], Part VII.

Comparing to the lattice Hamiltonian (2.17) of Chapter 2, the modes 1 and 2 can be identified with some modes $\mathbf{n}$ and $\mathbf{m}$, respectively. Then, $\omega_{12} = \omega_{\mathbf{nm}}/\chi$, while χ, $\omega_{\mathbf{nn}}$, and $\omega_{\mathbf{mm}}$ have been scaled out or moved into the Heisenberg evolution of the $\widehat{a}_j$. It has been assumed that $\omega_{\mathbf{nm}}$ is real, and that all $\gamma_{\mathbf{n}}$ and $\varepsilon_{\mathbf{n}} = 0$.

From the gauge P equations (5.17) of Chapter 5, and not yet specifying the exact form of the noise matrices, one obtains gauged Ito stochastic equations

$$d\alpha_j = -i\omega_{12}\alpha_{\neg j}\,dt - 2i\alpha_j^2\beta_j\,dt + \sum_k B_{jk}^{(\alpha)}(dW_k - \mathcal{G}_k\,dt) \tag{8.2a}$$

$$d\beta_j = i\omega_{12}\beta_{\neg j}\,dt + 2i\alpha_j\beta_j^2\,dt + \sum_k B_{jk}^{(\beta)}(dW_k - \mathcal{G}_k\,dt) \tag{8.2b}$$

$$d\Omega = \sum_k \mathcal{G}_k\,dW_k, \tag{8.2c}$$

where $\neg j = 1 + \delta_{1j}$, and dW_k are the usual Wiener increments. The noise matrices obey

$$\sum_l B_{jl}^{(\alpha)}B_{jk}^{(\alpha)} = -2i\delta_{jk}\alpha_j^2 \tag{8.3a}$$

$$\sum_l B_{jl}^{(\beta)}B_{jk}^{(\beta)} = 2i\delta_{jk}\beta_j^2 \tag{8.3b}$$

$$\sum_l B_{jl}^{(\alpha)}B_{jk}^{(\alpha)} = 0. \tag{8.3c}$$

Applying the drift and diffusion gauges (7.105) and (7.107) worked out in Chap-

ter 7 to each mode separately, these equations become

$$d\alpha_j = -i\omega_{12}\alpha_{\neg j}\,dt - 2i\alpha_j \mathrm{Re}\left\{\breve{n}_j\right\}\,dt + i\alpha_j\sqrt{2i}\left[\cosh g_j'' dW_{j1} + i\sinh g_j'' dW_{j2}\right] \quad (8.4a)$$

$$d\beta_j = i\omega_{12}\beta_{\neg j}\,dt + 2i\beta_j \mathrm{Re}\left\{\breve{n}_j\right\}\,dt + \beta_j\sqrt{2i}\left[-i\sinh g_j'' dW_{j1} + \cosh g_j'' dW_{j2}\right] \quad (8.4b)$$

$$d\Omega = -\sqrt{2i}\Omega\sum_j \mathrm{Im}\left\{\breve{n}_j\right\} e^{-g_j''}(dW_{j1} - i dW_{j2}), \quad (8.4c)$$

where $\breve{n}_j = \alpha_j\beta_j$, and

$$g_j'' = \frac{1}{6}\log\left\{8|\breve{n}_j|^2 t_{\mathrm{opt}} + (1 + 4\,\mathrm{Im}\left\{\breve{n}_j\right\}^2)^{3/2}\right\}. \quad (8.5)$$

The four independent real Wiener increments dW_{jk} can be implemented by independent Gaussian random variables of variance dt at each time step.

Proceeding to check the no-moving-singularities condition (6.3) as for the single mode in Section 7.3, there is no super-exponential growth of any $|\alpha_j|$, $|\beta_j|$ or $|\Omega|$. Moving singularities or noise divergences will not occur.

Two kinds of initial conditions were numerically investigated in detail:

8.2 Case 1: Coupling to a vacuum mode

8.2.1 Description

The system starts initially with a coherent state of mean particle number n_0 in mode 1, and vacuum in mode 2. In all simulations of this case, the inter-mode coupling strength was taken to be $\omega_{12} = 5$, but the mean particle number n_0 was varied. This mean particle number $\overline{N} = n_0 = \sum_j \langle\widehat{n}_j\rangle = \sum_j \langle\widehat{a}_j^\dagger\widehat{a}_j\rangle$ is conserved during each simulation.

At low particle number, the Rabi oscillations dominate the Hamiltonian, and particles oscillate between the modes, without much decoherence. At high particle number n_0, on the other hand, phase decoherence dominates mode 1, suppressing also the coherent transfer of particles to mode 2.

The particular values chosen to simulate were

$$n_0 = \{1, 17, 200, 1500, 10^4\}. \quad (8.6)$$

The two observables considered were: The fraction of particles in the (initially empty) mode 2:

$$p_2 = \frac{\langle \widehat{n}_2 \rangle}{\overline{N}}, \tag{8.7}$$

and the local normalized second order correlation functions of modes j:

$$g_j^{(2)}(t,t) = \frac{\langle : \widehat{n}_j(t) : \rangle}{\langle \widehat{n}_j(t) \rangle} = \frac{\langle \widehat{n}_j^2 \rangle}{\langle \widehat{n}_j \rangle^2} - \frac{1}{\langle \widehat{n}_j \rangle}. \tag{8.8}$$

The latter quantify the amount of (instantaneous) bunching/antibunching in the boson field, and for example, are unity for coherent states, two for thermal fields, and $1 - 1/n$ for Fock number states of n particles. Large values $g^{(2)} > 2$ occur e.g. for quantum superpositions of vacuum and Fock number states with two or more particles where the average particle number is small. For example in the state $|\psi\rangle = \sin\theta\,|0\rangle + \cos\theta\,|n\rangle$, $g^{(2)} = (1 - \frac{1}{n})/\cos^2\theta$.

8.2.2 Procedure

Three gauge choices were compared for this case.

1. *No gauge.* i.e. positive P.

2. *Drift and diffusion gauges* as in equations (8.4) with (8.5).The target time $t_{\rm opt}$ was varied to obtain the longest useful simulation time $t_{\rm sim}$.

3. *Drift gauge* (7.99) of Carusotto *et al*[1]. As pointed out before, a subtle difference from Ref. [1] is that here particle number conservation is not explicitly hardwired into the simulation, but happens to arise because no environment interactions are included in this particular simulation. This freedom is left unconstrained to make conclusions reached on the basis of the two modes relevant to a larger open many-mode system.

In each run, $\mathcal{S} = 2 \times 10^5$ trajectories were used, and useful simulation precision was defined as in (7.88), and simulation time $t_{\rm sim}$ accordingly.

In Figure 8.1 actual simulation times are compared to physical timescales and expected simulation times based on the single-mode analysis of Chapter 7. Note that

fitting parameters to (7.89) for the Carusotto *et al*[1] gauge (7.99) were calculated from single-mode simulations to be

$$\{c_0, \ldots, c_4\} = \{1, 3.3 \pm 0.5, 0.9\,^{+\infty}_{-0.2}, -0.3 \pm 0.4, 0.31 \pm 0.09\}, \tag{8.9}$$

and for (7.105) with (8.5) and $t_{\rm opt} = 0$ were

$$\{c_0, \ldots, c_4\} = \{1, 400 \pm 130, 3.6\,^{+\infty}_{-2.3}, 1.2 \pm 0.2, 0.42 \pm 0.03\}. \tag{8.10}$$

Example simulations are shown in Figures 8.2, 8.3, 8.4, and 8.5, and dependence of $t_{\rm sim}$ on the target time parameter $t_{\rm opt}$ are shown in Figure 8.6.

Any data from positive P simulations after the onset of spiking (numerical signature of possible boundary term errors) were discarded. The simulations up to such a point, showed no sign of any systematic biases[1].

8.2.3 Features seen

- With the single-mode gauge choices (7.105) and (8.5) applied directly to the twin-mode system, improvement over the positive P and Carusotto *et al* gauge (7.99)[1] is seen for all n_0
- This improvement becomes more and more significant at high mode occupations, like in the single-mode system. Generally speaking, the proportions between the simulation times obtained with the different gauge methods are qualitatively similar to the single-mode situation.
- At large mode occupations, one can still simulate well beyond coherence times, so most interesting phenomena should not be missed (apart from quantum revivals, of course). (See Figures 8.4–8.5)
- However, simulation times with all methods are significantly smaller than those predicted (by using expected mode occupation n_0) for single modes from Tables 7.1 or 7.2, or (8.9)–(8.10).

[1]The onset of spiking naturally moves to slightly earlier times as larger ensembles of trajectories are simulated. This may cause a beneficial "bias-concealing" effect in the following sense: As precision increases due to larger $\mathcal{S}$, some small boundary term biases that were originally concealed by noise might emerge, but simultaneously some rare trajectories with earlier spikes become included in the larger ensemble. These then warn one to discard data from an earlier time than one would have with the original smaller ensemble.

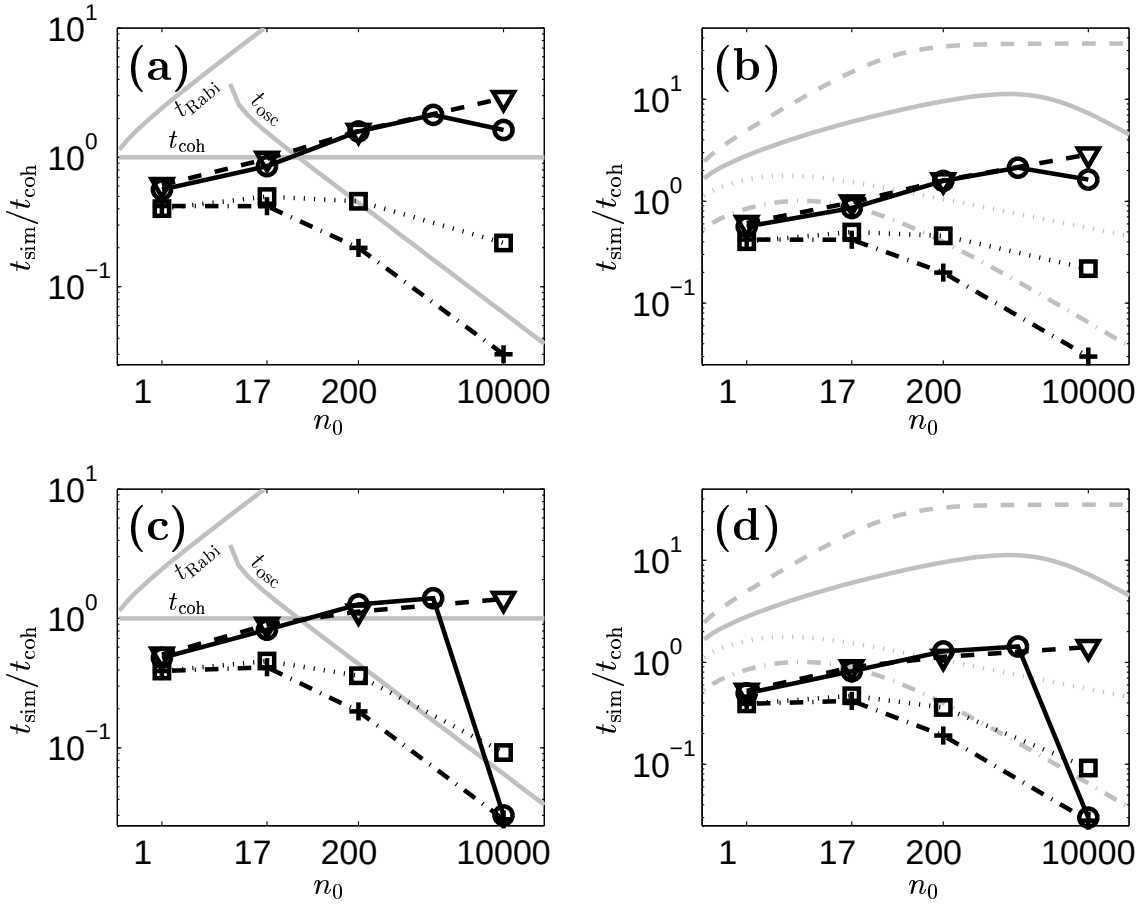

Figure 8.1: **Useful simulation times** $t_{\rm sim}$ for a mode coupled to vacuum as in Section 8.2. Calculated simulation times are shown as data points, with the symbols denoting gauge used. "□": positive P; "◯": drift gauge (7.105) and diffusion gauge (8.5) with $t_{\rm opt} = 0$; "+" drift gauge (7.99) of Carusotto *et al*[1]; "▽": drift and diffusion gauges (7.105) and (8.5) with best target time parameters: $\omega_{12}t_{\rm opt} = \{2.5, 0.5, 0.5, 0.075\}$ for $n_0 = \{1, 17, 200, 10^4\}$, respectively. Subplots **(a)** and **(b)** show simulation times based on estimates of the observable p_2, while **(c)** and **(d)** times based on $g_2^{(2)}$. Subplots **(a)** and **(c)** compare to physical time scales, including Rabi oscillation period $t_{\rm Rabi} = 2\pi/\omega_{12}$, while subplots **(b)** and **(d)** compare to expected simulation times for a single mode using the empirical fits of Table 7.2 and (8.9)–(8.10). The expected $t_{\rm sim}$ are plotted as light lines: DOTTED: positive P; SOLID: drift gauge (7.105) and diffusion gauge (8.5) with $t_{\rm opt} = 0$; DASHED: with optimum $t_{\rm opt}$ choice; DASH-DOTTED: drift gauge (7.99) of Carusotto *et al*[1].

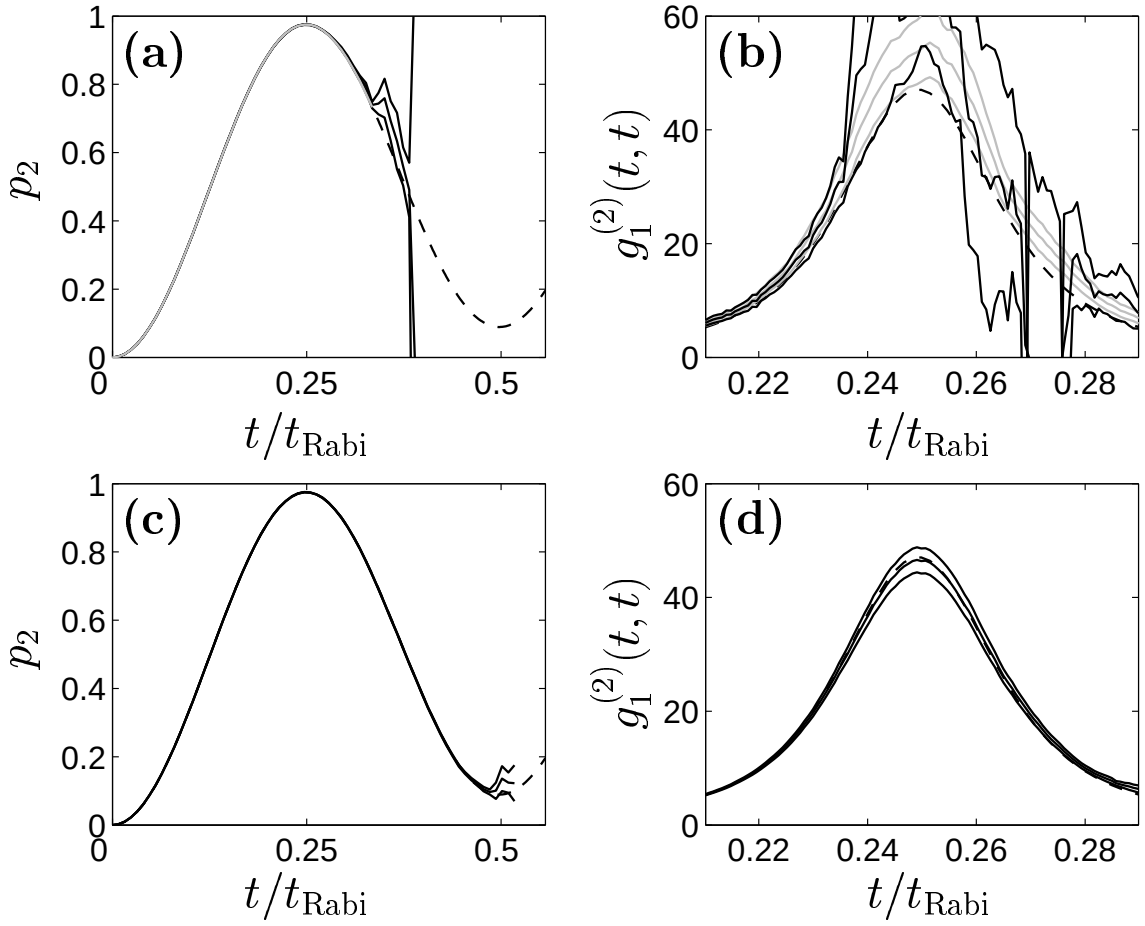

Figure 8.2: Coupling to vacuum mode: **System with few particles on average** ($n_0 = 1$). Time scaled to Rabi period $t_{\mathrm{Rabi}} = 2\pi/\omega_{12}$. Subfigures **(a)** and **(c)** show mode 2 particle fraction, while **(b)** and **(d)** show instantaneous particle number correlations in mode 2. Subfigures **(a)** and **(b)** show results with positive P LIGHT SOLID and drift gauge (7.99) DARK SOLID, whereas **(c)** and **(d)** show results with combined drift gauge (7.105) and diffusion gauge (7.107) using target time $t_{\mathrm{opt}} = 2.5/\omega_{12} \approx 0.4 t_{\mathrm{Rabi}}$. Exact results also shown (dashed). Triple lines indicate mean and error bars.

- No biases from the exact solution are seen for the cases ($n_0 = 1, 17$) where this was compared.

- The $n_0 = 17$ case was also simulated by Carusotto *et al*[1] with (solely) the drift gauge (7.99), and a simulation time of $\approx 0.55/\omega_{12}$ was seen. This is about 20% longer than with the same gauge here. This effect is most likely because there total particle number conservation was *a priori* imposed on each

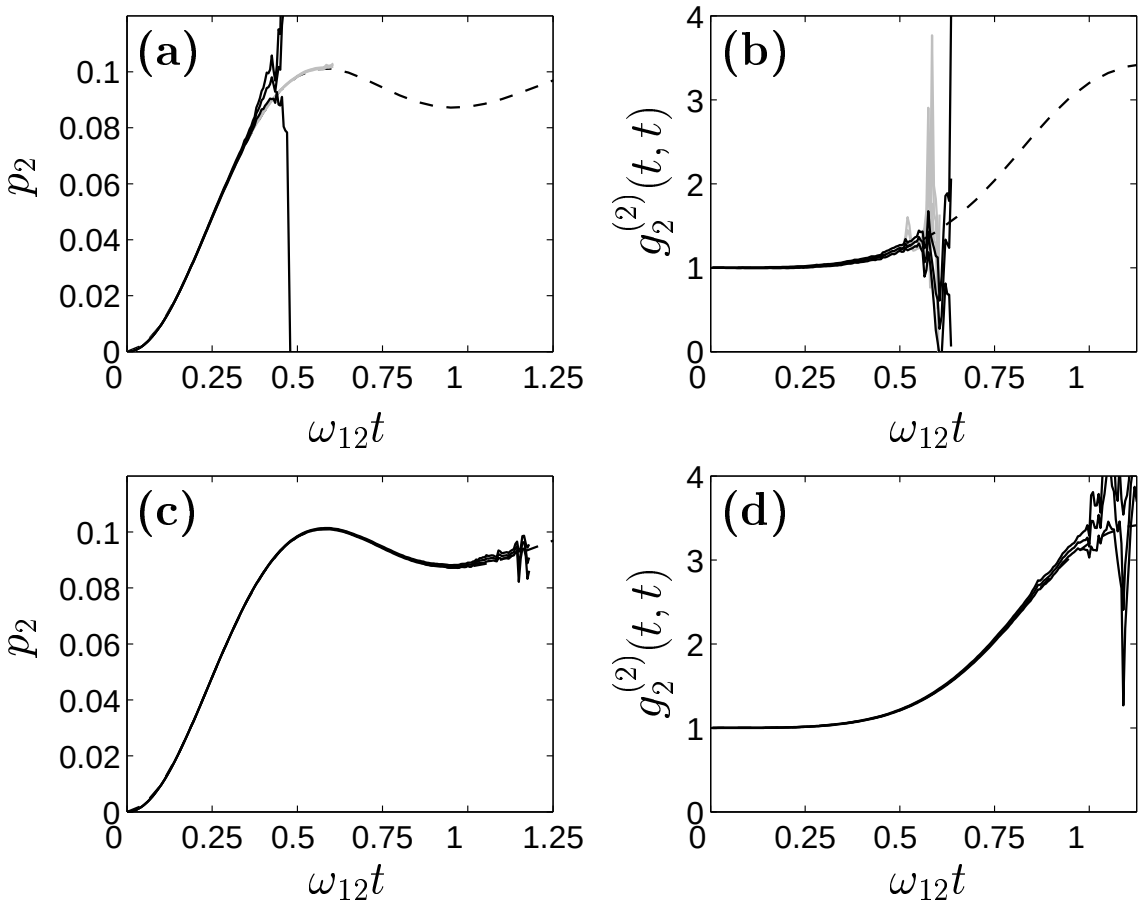

Figure 8.3: Coupling to vacuum mode:**System with intermediate number of particles** ($n_0 = 17$). Subfigures **(a)** and **(c)** show mode 2 particle fraction, while **(b)** and **(d)** show instantaneous particle number correlations in mode 2. Subfigures **(a)** and **(b)** show results with positive P LIGHT SOLID and drift gauge (7.99) DARK SOLID, whereas **(c)** and **(d)** show results with combined drift gauge (7.105) and diffusion gauge (7.107) using target time $\omega_{12}t_{\rm opt} = 0.5$. Exact results also shown (dashed). Triple lines indicate mean and error bars.

trajectory rather than only in the ensemble mean as here. The extra freedom in the present simulations is necessary to allow straightforward extension to open systems, but the price paid appears to be some extra inefficiency.

- Precision in the highly-occupied mode appears largely insensitive to the choice of target time $t_{\rm opt}$, as long as it is within reasonable values (See Figure 8.6). A choice of $t_{\rm opt} = 0$ achieves very large improvement over positive P and drift-gauge only simulations for these observables. Note that $t_{\rm opt} = 0$ is not the same as no diffusion gauge, because (8.5) becomes $g_j'' = \frac{1}{4}\log(1 + 4\mathrm{Im}\{\breve{n}_j\}^2)$,

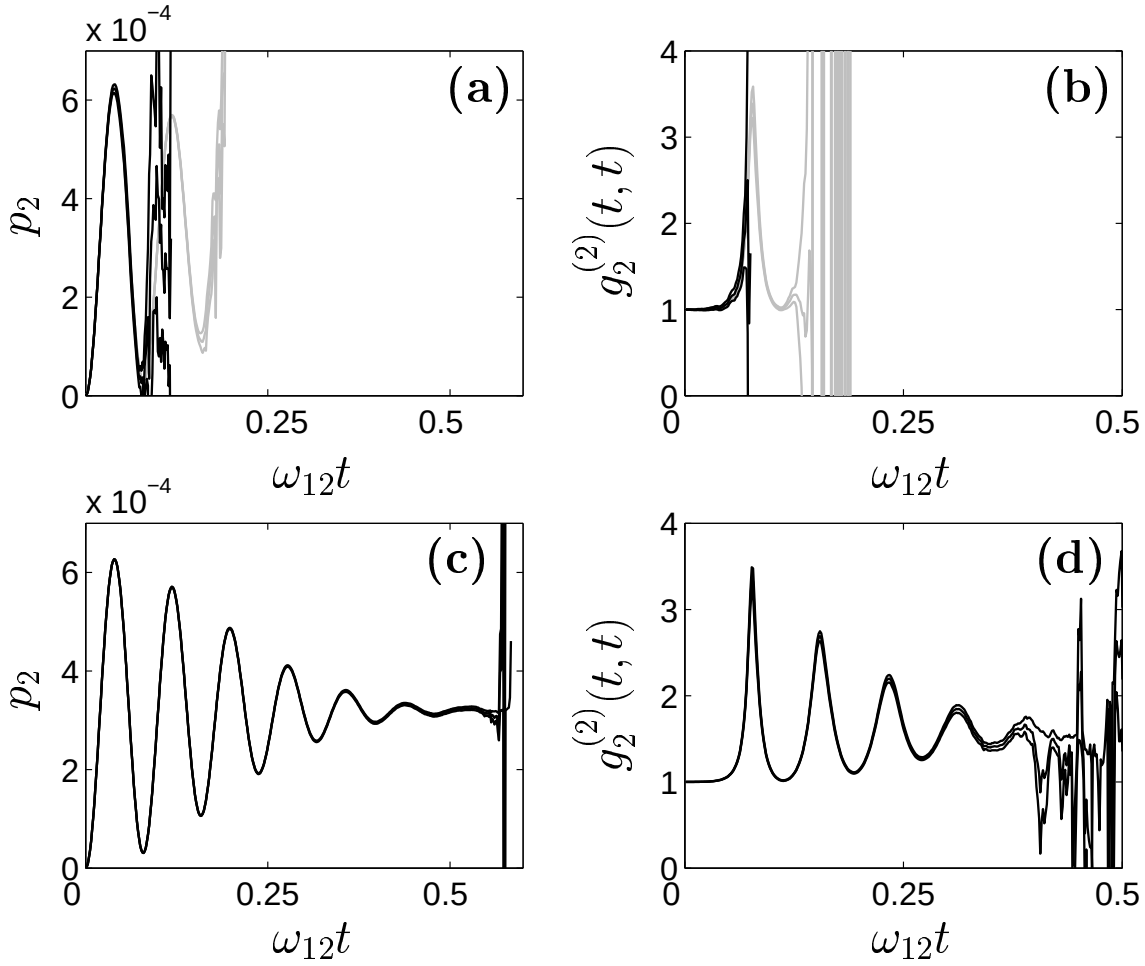

Figure 8.4: Coupling to vacuum mode: **System with large number of particles** ($n_0 = 200$). Subfigures **(a)** and **(c)** show mode 2 particle fraction, while **(b)** and **(d)** show instantaneous particle number correlations in mode 2. Subfigures **(a)** and **(b)** show results with positive P LIGHT SOLID and drift gauge (7.99) DARK SOLID, whereas **(c)** and **(d)** show results with combined drift gauge (7.105) and diffusion gauge (7.107) using target time $\omega_{12}t_{\rm opt} = 0.25$. Triple lines indicate mean and error bars.

and this appears to have an important effect. The same applies to mode 2 when n_0 is not large.

- At high n_0 the observables for the nearly-vacuum mode 2 become sensitive to target time choice (See Figure 8.6). This is particularly evident for $g_2^{(2)}$ when $n_0 = 10^4$. The optimum target time $t_{\rm opt}$ is then sharply peaked, much as in the single-mode case, and $t_{\rm sim} \approx\geq t_{\rm opt}$ in the optimum region where $t_{\rm opt}$ is of the order of coherence time for the highly-occupied mode 1.

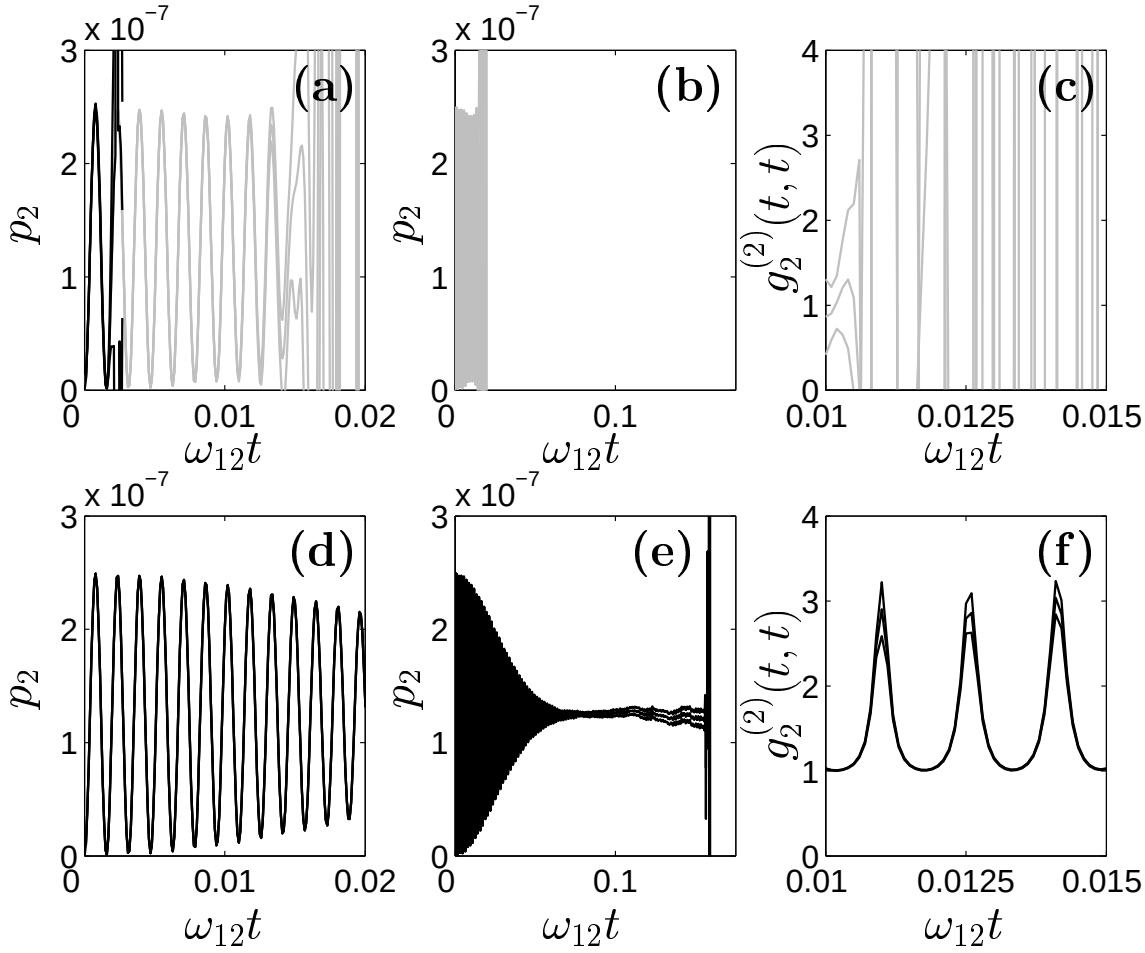

Figure 8.5: Coupling to vacuum mode: **System with very large number of particles** ($n_0 = 10^4$). Subfigures **(a)**, **(b)**, **(d)** and **(e)** show mode 2 particle fraction, while **(c)** and **(f)** show instantaneous particle number correlations in mode 2. Subfigures **(a)**–**(c)** show results with positive P LIGHT SOLID and drift gauge (7.99) DARK SOLID, whereas **(d)**– **(f)** show results with combined drift gauge (7.105) and diffusion gauge (7.107) using target time $\omega_{12}t_{\rm opt} = 0.1$. Triple lines indicate mean and error bars.

- One point to note is that "useful simulation time" $t_{\rm sim}$ was based on the moment when relative error in a quantity was *first* found to be too large. In calculations of $g^{(2)}$, uncertainties are much greater when $g^{(2)}(0,t)$ peaks — see e.g. Figure 8.5**(f)**. Good accuracy can often be obtained between peaks for much longer times than shown in Figure 8.6, up to about the same simulation time as worked out based on the occupation number. This is particularly evident in the $n_0 = 10^4$ case, where the sudden drop-off in $t_{\rm sim}$ is due to this

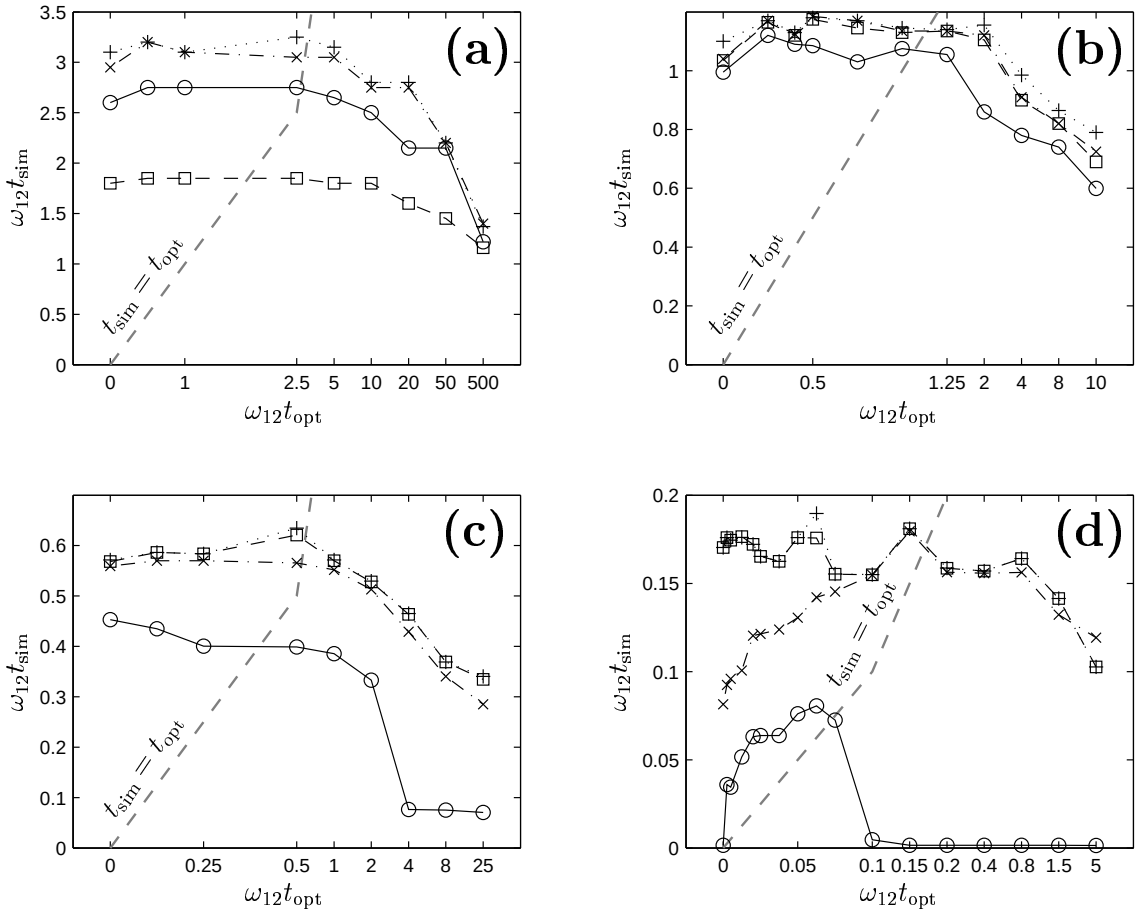

Figure 8.6: Dependence of **useful simulation time** $t_{\rm sim}$ on the target time parameter $t_{\rm opt}$ for simulations of Section 8.2 "+": useful simulation of $\langle \widehat{n}_1 \rangle$, "×": of $\langle \widehat{n}_2 \rangle$, "□": of $g_1^{(2)}$, "◯": of $g_2^{(2)}$. Nonlinear but monotonic $t_{\rm opt}$ scale used to avoid overlap of data points, while showing trend. Subplot **(a)**: $n_0 = 1$; **(b)**: $n_0 = 17$; **(c)**: $n_0 = 200$; **(d)**: $n_0 = 10^4$. $t_{\rm opt} = t_{\rm sim}$ shown for reference as LIGHT DASHED line.

effect (see solid line of Figure 8.6**(d)**).

- Best simulation times at high n_0 occur for $t_{\rm opt} \leq \approx t_{\rm sim}$.
- Positive P simulations do better than those based on the drift gauge (7.99) for all n_0.
- Best simulation times (based on $\langle \widehat{n}_2 \rangle$) with both gauges appear to scale roughly as

$$\omega_{12} t_{\rm sim} \approx 3/n_0^{1/3} \tag{8.11}$$

Collective conclusions are left till the end of the chapter.

8.2.4 Comparison to Fock state stochastic wavefunctions

The simulation of a seemingly similar 17-particle two-mode system was carried out by Carusotto *et al*[1] using the "simple Fock state scheme" with stochastic wavefunctions. This method gave a useful simulation time of $\approx 3/\omega_{12}$ with $\mathcal{S} = 2 \times 10^5$ trajectories. This is longer than seen with either the "simple coherent state scheme" therein ($\approx 0.55/\omega_{12}$), or the simulation in Figure 8.3 here ($\approx 1.18/\omega_{12}$). This was, however, for number-state initial conditions, so the two types of simulation cannot be easily directly compared, and the observable expectation values calculated are different.

Coherent states with mean occupation n_0, used as starting points here, contain Fock components with much larger numbers of particles than n_0. Since the spread in the norm, and hence the uncertainty of observables, has been found to rise exponentially depending on the quantity $\overline{N}t = n_0 t$ (from equation (78) in [1]), one expects that useful simulation time of the simple Fock state scheme will be $\approx\propto 1/\overline{N} = 1/n_0$. This is a sharp decrease compared to the $1/n_0^{1/3}$ dependence with the combined gauges discussed here, and one expects that for $n_0 \gg 17$, the Fock state wavefunction method will give much shorter simulation times.

One can attempt to compare schemes for $n_0 = 17$ in spite of the differences in the physical system simulated. It is not clear how best to sample a coherent state (which includes Fock state components with different particle numbers) with the Fock scheme, but one can estimate that for accuracy one should consider components with occupation at least three standard deviations away from the mean giving $\overline{N} \lesssim 30$ for such Fock state components. A trajectory corresponding to such a component might be expected to not diverge for times $\omega_{12} t \lesssim 1.7$.

This is about 30% longer than seen in Figure 8.3, a factor similar to that noticed between simulations using the gauge (7.99) in Ref. [1] using the "simple coherent scheme" and here. It is likely the price paid for having the formalism left open to simulating gains and losses.

8.3 Case 2: Coherent mixing of two identical modes

8.3.1 Description

The system starts initially with identical coherent states of mean particle number n_0 in each mode. The total mean particle number is $\overline{N} = 2\,n_0$. During time evolution, Rabi coupling of the modes occurs along with some decoherence from inter-atom collisions in each mode. This time simulations were carried out with constant particle number $n_0 = 100$, but the coupling frequency ω_{12} was varied.

At low frequency $\omega_{12} \ll n_0 = 100$, decoherence local to each mode dominates, and phase oscillations in each mode occur with period $t_{\rm osc} = \pi/n_0$, while at high frequency $\omega_{12} \gg n_0 = 100$, the inter-mode coupling dominates and phase oscillations for each mode occur with period $2\pi/\omega_{12}$. One expects that for low coupling the two modes should behave largely as two independent single modes of Chapter 7.

The particular values chosen to simulate were

$$\omega_{12} = \{5000, 500, 50, 5, 0.5, 0.05, 0.005, 0.0005\}. \tag{8.12}$$

The observable of most interest here was $G^{(1)}(0,t)$ as in the single-mode case. Due to the symmetry of the system, all single-mode observables such as this have identical expectation values for both modes, so either mode can be considered.

The procedure was the same here as outlined in Section 8.2.2, with $\mathcal{S} = 10^4$ trajectories per simulation.

In Figure 8.7 actual simulation times are compared to physical timescales and expected simulation times based on the single-mode analysis of Chapter 7. Simulation times $t_{\rm sim}$ were based on the condition (7.88) for the observable $|G^{(1)}(0,t)|$.

Figure 8.8 shows data from a quick search for optimum target times $t_{\rm opt}$, while some example simulations are shown in Figures 8.9, 8.10, and 8.11.

8.3.2 Features seen

- At weak coupling $\omega_{12} \ll n_0$, the simulation times with various gauge choices behave qualitatively similar to the single mode of Chapter 7, and vacuum

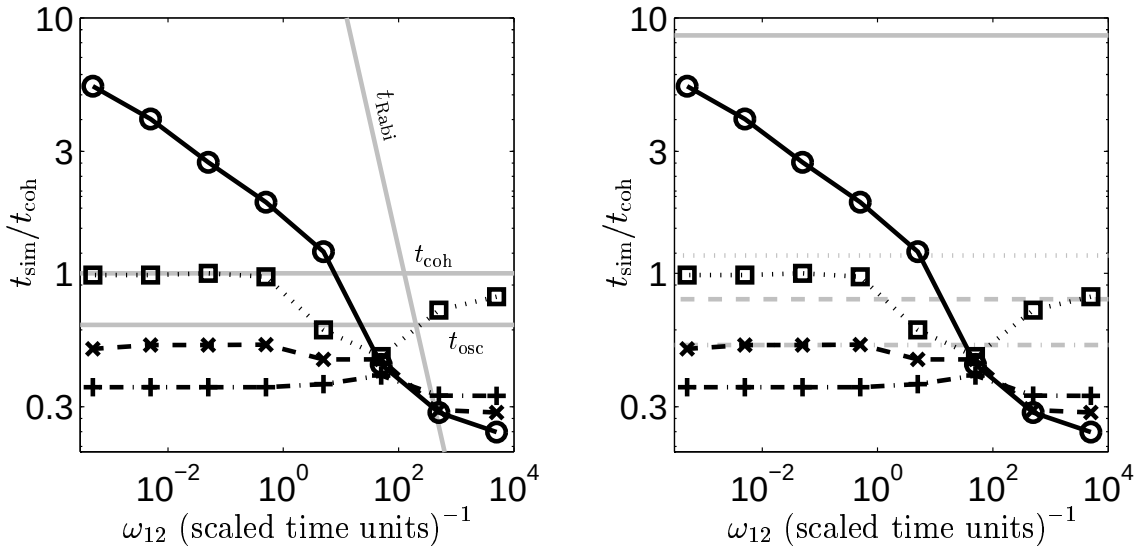

Figure 8.7: **Useful simulation times** $t_{\rm sim}$ for a two identical modes undergoing coherent mixing as in Section 8.3. Calculated simulation times are shown as data points, with the symbols denoting gauge used. "□": positive P; "◯": drift gauge (7.105) and diffusion gauge (8.5) with $t_{\rm opt} = 0$; "+" drift gauge (7.99) of Carusotto *et al*[1]; "×": drift gauge (7.105) only. Subplot **(a)** compares to physical time scales, including Rabi oscillation period $t_{\rm Rabi} = 2\pi/\omega_{12}$, while subplot **(b)** compares to expected simulation times for a single mode using the empirical fits of Table 7.2 and (8.9)–(8.10). The expected $t_{\rm sim}$ are plotted as light lines: DOTTED: positive P; SOLID: drift gauge (7.105) and diffusion gauge (8.5) with $t_{\rm opt} = 0$; DASHED: with drift gauge (7.105) only; DASH-DOTTED: drift gauge (7.99) of Carusotto *et al*[1].

coupled modes of Section 8.2. That is, the dual gauge combination (7.105) and (8.5) allows simulation until the system has decohered, and give much longer simulation times than the positive P, drift gauge (7.105) only, or Carusotto *et al* gauge (7.99) (in that order). The drift-gauge-only methods simulate for less time than a single phase oscillation period.

- Simulation times are shorter for all methods than those given in Table 7.1 for the relevant single-mode case.

- At strong coupling, $\omega_{12} \gg n_0$, the plain positive P method appears to give the best results out of the gauges tried. The times achievable with the gauged methods are much shorter. Relatively longest with the Carusotto *et al* gauge

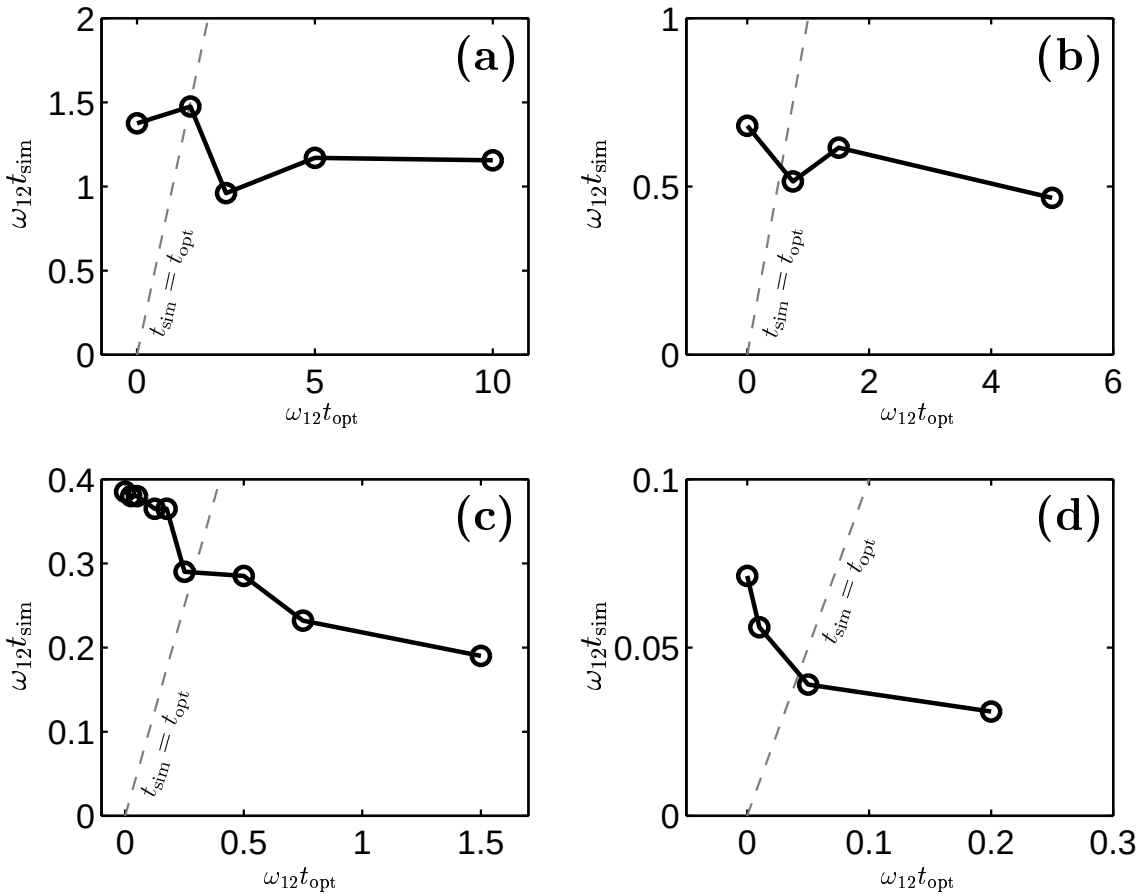

Figure 8.8: Mixing of two identical modes: Dependence of **useful simulation time** $t_{\rm sim}$ on the target time parameter $t_{\rm opt}$ for simulations of Section 8.3. Subplots **(a)** to **(d)** are for coupling strengths $\omega_{12} = \{0.0005, 0.05, 5, 500\}$, respectively. Data are from single simulations with $\mathcal{S} = 10^4$.

(7.99), then the drift gauge (7.105), and worst performance is obtained from the diffusion-gauged simulation.

- At strong coupling, none of the methods tried reach coherence time $t_{\rm coh}$, but many Rabi oscillations can be simulated by all methods, since these are now much shorter than $t_{\rm osc}$.

- Choosing various target times $t_{\rm opt}$ appears not to have no effect apart from a worsening of the simulation at large $t_{\rm opt}$ values. Note that this was also the situation for the vacuum-coupled simulations in Section 8.2 with the same total particle number $\overline{N} = 200$, and so this lack of improvement with $t_{\rm opt}$ may be typical of lower mode occupations when any significant coupling ω_{12}

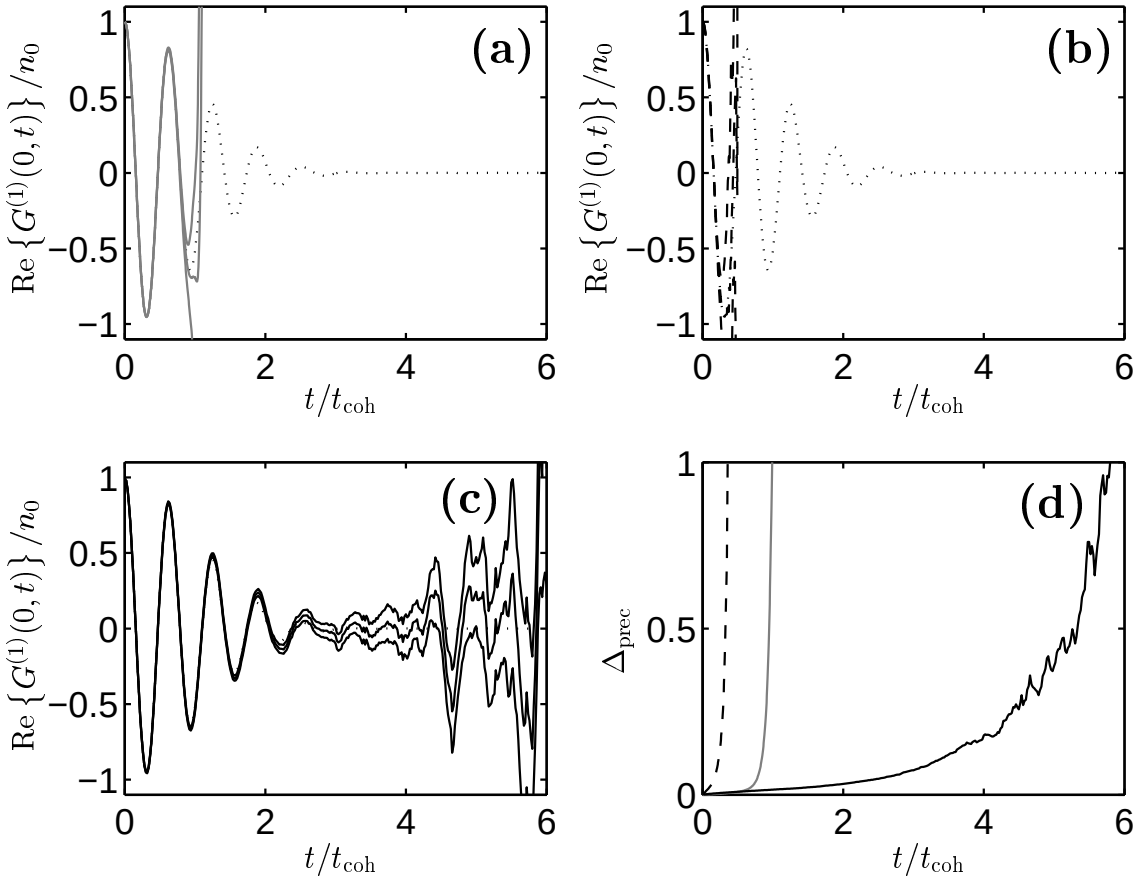

Figure 8.9: Mixing of two identical modes: **Weak coupling:** ($\omega_{12} = 0.0005$). Subplots **(a)**–**(c)** show, respectively, simulations with positive P (LIGHT LINE); with Carusotto *et al*[1] drift gauge (7.99) (DASHED LINE); and with both drift gauge (7.105) and diffusion gauge (8.5) (SOLID LINE). The exact solution (7.11b) for no coupling ($\omega_{12} = 0$) is shown as a DOTTED LINE. Subplot **(d)** shows relative sampling error in the estimate of $|G^{(1)}(0,t)|$, such that $\Delta_{\mathrm{prec}} = 10\sqrt{\mathcal{S}/10^6}\Delta|G^{(1)}(0,t)|/|G^{(1)}(0,t)$ is less then unity while "useful" precision is present, when defined as in (7.88).

---

is present.

- At strong coupling, the Carusotto *et al*gauge (7.99) allowed somewhat longer simulation times, while the signal to noise ratio in the estimate of $G^{(1)}(0,t)$ was lower with the gauge (7.105) at short and intermediate times — see Figure 8.11**(d)**.

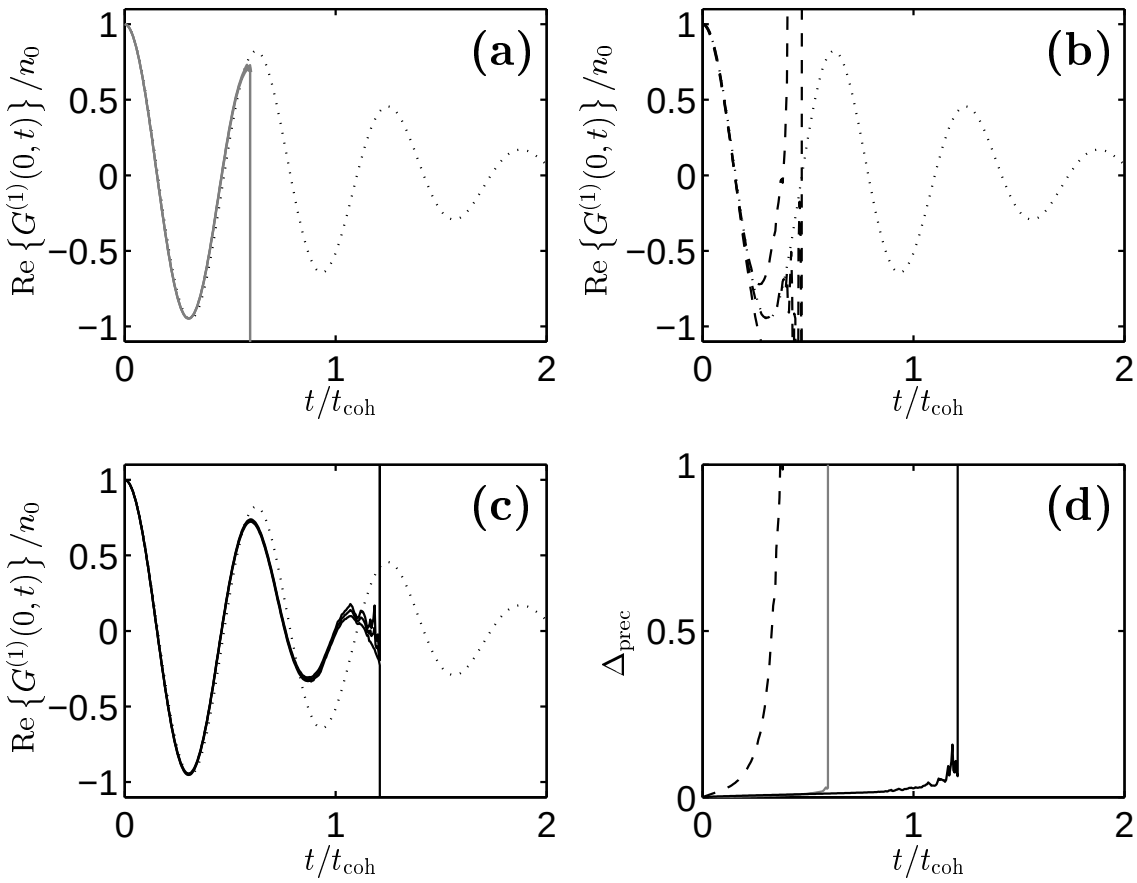

Figure 8.10: Mixing of two identical modes: **Intermediate coupling:** ($\omega_{12} = 5$). Subplots **(a)**–**(c)** show, respectively, simulations with positive P (LIGHT LINE); with Carusotto *et al*[1] drift gauge (7.99) (DASHED LINE); and with both drift gauge (7.105) and diffusion gauge (8.5) (SOLID LINE). The exact solution (7.11b) for no coupling ($\omega_{12} = 0$) is shown as a DOTTED LINE. Subplot **(d)** shows relative sampling error in the estimate of $|G^{(1)}(0,t)|$, such that $\Delta_{\mathrm{prec}} = 10\sqrt{\mathcal{S}/10^6}\Delta|G^{(1)}(0,t)|/|G^{(1)}(0,t)$ is less then unity while "useful" precision is present, when defined as in (7.88).

8.4 Analysis and Conclusions

The two kinds of initial conditions considered above represent the two kinds of situations generically occurring in all many-mode simulations. Coupling between modes of widely differing occupation will lead to behavior similar to that seen in Section 8.2 (Case 1). Coupling between modes of similar occupation will display features similar to those seen in Section 8.3 (Case 2). Adjacent spatial or momentum modes typically behave like Case 2, since if a field model is well resolved by the

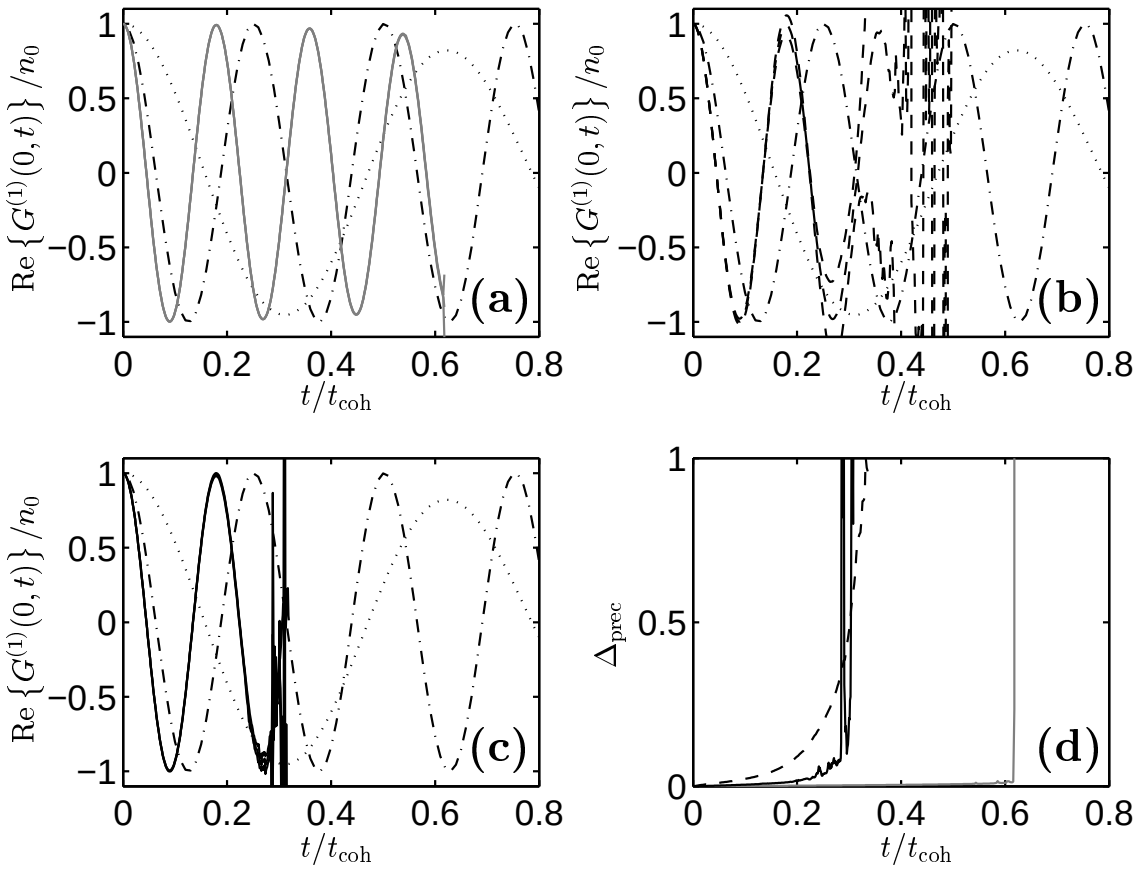

Figure 8.11: Mixing of two identical modes: **Strong coupling:** ($\omega_{12} = 500$). Subplots **(a)**–**(c)** show, respectively, simulations with positive P (LIGHT LINE); with Carusotto *et al*[1] drift gauge (7.99) (DASHED LINE); and with both drift gauge (7.105) and diffusion gauge (8.5) (SOLID LINE). The exact solution for (7.11b) no coupling ($\omega_{12} = 0$) is shown as a DOTTED LINE, and for no collisions ($\omega_{12} \to \infty$) as a DOT-DASHED LINE. Subplot **(d)** shows relative sampling error in the estimate of $|G^{(1)}(0,t)|$, such that $\Delta_{\mathrm{prec}} = 10\sqrt{\mathcal{S}/10^6}\Delta|G^{(1)}(0,t)|/|G^{(1)}(0,t)$ is less then unity while "useful" precision is present, when defined as in (7.88).

lattice, then physical properties (e.g. density, and hence mode occupation) should not change much over the distance between neighboring lattice points.

Still, this chapter has not really been a comprehensive assessment of gauge performance for all coupled mode cases, since not all parameter regimes have been explored. For the most general two modes starting in (off-diagonal) coherent state initial conditions one could be looking at the 5 complex parameters $\breve{n}_j$, α_j, ω_{12} — no mean feat to investigate. Rather, this chapter has been a study of several commonly occurring cases to get an indication of whether the simulation improvements found

for a single mode survive when inter-mode coupling is present, and to what degree.

Several aspects of the situation have emerged:

1. When scattering within a mode dominates over the coupling between modes, the response of the system to the gauges is similar to what was seen for a single mode. That is,

   (a) When mode occupation is high $\breve{n}_j \gg 1$, use of the combined drift (7.105) and diffusion (8.5) gauges developed in Chapter 7 gives dramatic improvement in useful simulation times and observable precision over the positive P method. In this regime, the drift-gauged only (e.g. (7.105) or (7.99)) simulations reduce simulation time from even the positive P case, although boundary terms are removed. Using both gauges (7.105) and (8.5) allows simulation to times by which full decoherence has occurred.

   (b) When mode occupation is low $n_0 \lesssim \mathcal{O}(1)$, the improvement gained with the gauges is smaller although some improvement is always seen. The absolute simulation time is longer than for $n_0 \gg 1$, however.

   Still, it turns out that in this strong scattering regime, one doesn't need much inter-mode coupling ω_{12} to reduce the simulation time in absolute terms by a factor $\mathcal{O}(2-10)$, although this reduction mainly affects the time after full decoherence has occurred, and not much is physically happening.

2. The beneficial effect of choosing $t_{\text{opt}} > 0$ appears to be strongly suppressed when the coupling ω_{12} is weak but not yet *very* weak, or the mode occupation is large but not yet *very* large. The $t_{\text{opt}} = 0$ diffusion gauge

$$g_j''(t_{\text{opt}} = 0) = \frac{1}{4}\log(1 + 4\text{Im}\{\breve{n}_j\}^2), \tag{8.13}$$

   does however have a marked beneficial effect whenever two body scattering is significant, and simulations using this gauge show very significant improvement over positive P or $g_j'' = 0$ simulations for a wide range of parameters. This parameter range appears to be $\omega_{12} \ll \breve{n}\chi$, and $\mathcal{O}(1) \lesssim n_0 \lesssim \mathcal{O}(10^3)$. Simulation times obtained are smaller by about a factor of $\mathcal{O}(2)$ than those

given for a single mode with the same gauge. At higher occupations, the benefit gained with (8.13) abates but nonzero $t_{\rm opt}$ values appear to become useful again, and continue to provide strong improvements over positive P simulations. (See, e.g. Figure 8.1**(d)**.) The gauge (8.13) is convenient also because there is no *a priori* parameter $t_{\rm opt}$.

3. When the inter-mode coupling dominates, the gauges developed in Chapter 7 or by Carusotto *et al*[1] do not appear to be very useful. They actually reduce simulation time as compared to the plain positive P method, although several Rabi oscillation periods can always be simulated.

   The transition between the strong and weak coupling behavior appears to be at around

$$\omega_{12} \approx \chi \breve{n}, \tag{8.14}$$

   which is the point at which the expectation values of the coupling and two-body scattering energies in the Hamiltonian are approximately equal.

At the level of the stochastic equations (8.2), the evolution of (say) $d\alpha_j$ can gather noise from three sources

1. Directly from the local noise term $\propto \alpha_j \sqrt{\chi}\, dW_j$
2. Indirectly from the local nonlinear term $\propto \chi \alpha_j \breve{n}_j$, which can amplify variation in the local noise term.
3. From the other mode through the coupling term $\propto \omega_{12} \alpha_{\neg j}$.

The drift gauges (7.105) developed here or (7.99) developed by Carusotto *et al*[1] neutralize source 2. The diffusion gauges (8.5) or (7.97d) suppresses the direct noise source 1. No local gauge can suppress the third source of randomness, however, because the randomness in $\alpha_{\neg j}$ is largely independent of any processes occurring in mode j. What happens is that even small randomness in one mode feeds into the other, can become amplified, and fed back again.

The part of the diffusion gauge that is retained at $t_{\rm opt} = 0$ appears more robust to this mixing than the additional optimization obtained with $t_{\rm opt} > 0$.

Based on this, and the behavior $t_{\rm sim}$ vs. $t_{\rm opt}$ shown e.g. in Figures 7.4 and 8.6, a way to proceed with a full many-mode simulation would be to

1. Run a simulation with local drift gauge (7.105), and $t_{\rm opt} = 0$ diffusion gauge (8.13). Call the simulation time obtained $t_{\rm sim}^{(0)}$.

2. Run a simulation with $t_{\rm opt} = t_{\rm sim}^{(0)}$, and obtain a simulation time $t_{\rm sim}^{(1)}$.

3. If $t_{\rm sim}^{(1)} > t_{\rm sim}^{(0)}$ then nonzero $t_{\rm opt}$ is be beneficial, one expects $t_{\rm sim} \gtrsim t_{\rm opt}$, and one can make a search for a reasonable value by now running a simulation with $t_{\rm opt} = t_{\rm sim}^{(1)}$, and iterating in this manner until no more significant improvement is gained.

   If, on the other hand, $t_{\rm sim}^{(1)} \lesssim t_{\rm sim}^{(0)}$, then it appears that one is in a regime where the $t_{\rm opt}$ parameter does not affect the dominant noise source, and $t_{\rm sim}^{(0)}$ is the best simulation time one can obtain with the (7.105)&(8.5) dual gauge method.

4. If simulation time is too short, it may be worth trying a plain positive P simulation, or even a diffusion-gauge-only simulation using (7.97d), while carefully monitoring for the presence of spiking, and discarding any data beyond the first spike time. (The simulations carried out in this chapter with this approach did not show any bias when compared with exact results — see e.g. Figures 8.2 and 8.3).

In conclusion, it has been found in this chapter that simulation time and precision improvement can still be gained with coupled modes by using the local drift and diffusion gauges (7.105) and (8.5), although marked improvement will mostly be seen only when two-particle scattering dominates the inter-mode coupling. Other non-local gauges may improve simulations in a regime where inter-mode coupling dominates but development of such is for future research.